CHEMISTRY
A EUROPEAN JOURNAL

FULL PAPER

DOI: 10.1002/chem.201200457

Cyclic RGD Peptidomimetics Containing Bifunctional Diketopiperazine Scaffolds as New Potent Integrin Ligands

Mattia Marchini,[a] Michele Mingozzi,[a] Raffaele Colombo,[a] Ileana Guzzetti,[a] Laura Belvisi,*[a] Francesca Vasile,[a] Donatella Potenza,[a] Umberto Piarulli,*[b] Daniela Arosio,[c] and Cesare Gennari*[a]

Abstract: The synthesis of eight bifunctional diketopiperazine (DKP) scaffolds is described; these were formally derived from 2,3-diaminopropionic acid and aspartic acid (**DKP-1**–**DKP-7**) or glutamic acid (**DKP-8**) and feature an amine and a carboxylic acid functional group. The scaffolds differ in the configuration at the two stereocenters and the substitution at the diketopiperazinic nitrogen atoms. The bifunctional diketopiperazines were introduced into eight cyclic peptidomimetics containing the Arg-Gly-Asp (RGD) sequence. The resulting RGD peptidomimetics were screened for their ability to inhibit biotinylated vitronectin binding to the purified integrins $\alpha_v\beta_3$ and $\alpha_v\beta_5$, which are involved in tumor angiogenesis. Nanomolar IC_{50} values were obtained for the RGD peptidomimetics derived from *trans* DKP scaffolds (**DKP-2**–**DKP-8**). Conformational studies of the cyclic RGD peptidomimetics by ^{1}H NMR spectroscopy experiments (VT-NMR and NOESY spectroscopy) in aqueous solution and Monte Carlo/Stochastic Dynamics (MC/SD) simulations revealed that the highest affinity ligands display well-defined preferred conformations featuring intramolecular hydrogen-bonded turn motifs and an extended arrangement of the RGD sequence [Cβ(Arg)–Cβ(Asp) average distance ≥8.8 Å]. Docking studies were performed, starting from the representative conformations obtained from the MC/SD simulations and taking as a reference model the crystal structure of the extracellular segment of integrin $\alpha_v\beta_3$ complexed with the cyclic pentapeptide, Cilengitide. The highest affinity ligands produced top-ranked poses conserving all the important interactions of the X-ray complex.

Keywords: conformation analysis · diketopiperazines · molecular modeling · peptides · peptidomimetics

Introduction

Integrins are a large family of transmembrane heterodimeric receptors that, once bound to extracellular matrix proteins, regulate a variety of cellular processes.[1] As a consequence of their role in important physiological phenomena, integrin defects have been implicated in many common diseases. Hence, it is not surprising that some integrins have become attractive targets for pharmacological intervention in a number of pathological conditions.[2] The observation that $\alpha_V\beta_3$, $\alpha_V\beta_5$ and $\alpha_5\beta_1$ integrin subtypes are essential for tumor angiogenesis and can be successfully inhibited by small-molecule ligands has turned them into the focus of cancer research.[3]

Across their extracellular α/β subunit interface containing the metal ion-dependent adhesion site (MIDAS), integrins recognize and bind protein ligands through contiguous tripeptide sequences, the majority of which are present within flexible loop regions and contain an acidic residue.[4] Several integrins, including $\alpha_5\beta_1$ and α_V integrins, recognize Arg-Gly-Asp (RGD) sequences in endogenous ligands. The context of the ligand RGD sequence (flanking residues, three dimensional presentation) and individual features of the integrin binding pockets determine the recognition specificity and efficacy. A major breakthrough for understanding this interaction at a molecular level came in 2002 when the X-ray structure of the complex of integrin $\alpha_V\beta_3$ with cyclo-[Arg-Gly-Asp-D-Phe-N(Me)-Val] (Cilengitide) was revealed.[5] This potent $\alpha_V\beta_3$ ligand was developed by Kessler and co-workers (Figure 1),[6,7] and is currently in phase III clinical trials as an angiogenesis inhibitor for patients with glioblastoma multiforme.[8] The high activity and selectivity of this derivative has been attributed to an extended confor-

[a] M. Marchini, M. Mingozzi, R. Colombo, I. Guzzetti, Dr. L. Belvisi, Dr. F. Vasile, Dr. D. Potenza, Prof. Dr. C. Gennari
Università degli Studi di Milano
Dipartimento di Chimica Organica e Industriale
Via Venezian, 21, I-20133, Milan (Italy)
Fax: (+39) 0250314072
E-mail: laura.belvisi@unimi.it
cesare.gennari@unimi.it

[b] Prof. Dr. U. Piarulli
Università degli Studi dell'Insubria
Dipartimento di Scienza e Alta Tecnologia
Via Valleggio 11, I-22100, Como (Italy)
Fax: (+39) 0312386449
E-mail: umberto.piarulli@uninsubria.it

[c] Dr. D. Arosio
CNR, Istituto di Scienze e Tecnologie Molecolari (ISTM)
Via Venezian, 21, I-20133, Milan (Italy)

Supporting information for this article is available on the WWW under http://dx.doi.org/10.1002/chem.201200457.

© 2012 Wiley-VCH Verlag GmbH & Co. KGaA, Weinheim

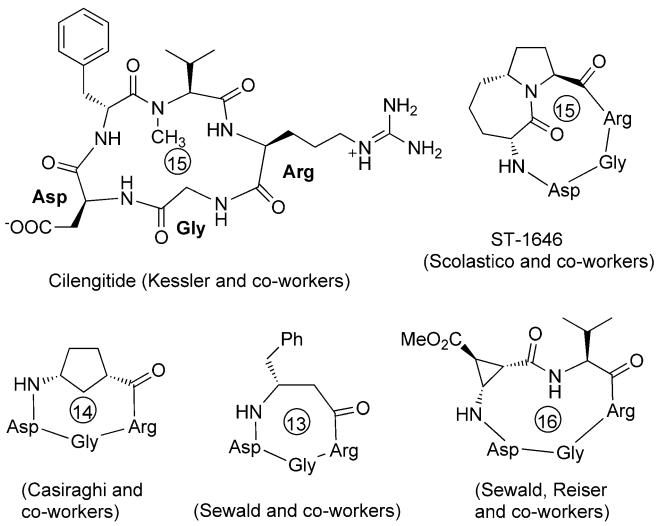

Figure 1. Potent $\alpha_v\beta_3$ ligands.

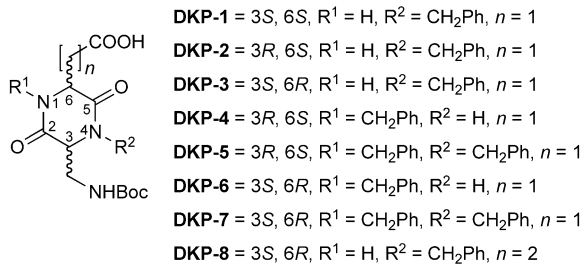

Figure 2. Bifunctional DKP scaffolds.

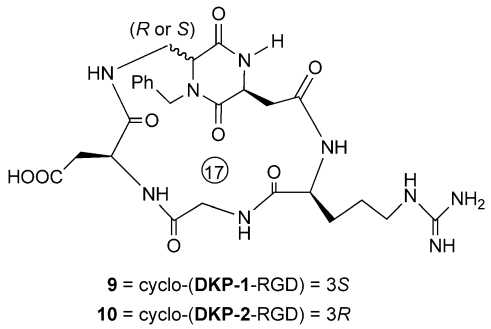

Figure 3. Cyclic RGD peptidomimetics containing bifunctional DKP scaffolds.

mation of the RGD motif displaying a distance of about 9 Å between the C_β atoms of Asp and Arg.[5]

These observations prompted many other research groups to investigate the use of conformationally constrained cyclic RGD peptides and peptidomimetics as active and selective integrin ligands, encompassing a wide variety of rigid scaffolds and featuring 13-, 14-, 15- and 16-membered rings (Figure 1).[9] Among the successful approaches, we would like to mention the γ-amino acid RGD peptidomimetics containing a γ-aminocyclopentane carboxylic acid or a 4-aminoproline residue (14-membered ring),[10] the azabicyclic lactam RGD peptidomimetics (15-membered ring, with the scaffold mimicking a constrained dipeptide, e.g., ST1646),[11] and the β-amino acid RGD peptidomimetics, embodying β^3-homoamino acids[12] (13-membered ring) or a *cis*-β-aminocyclopropane carboxylic acid (16-membered ring).[13] Up to now, a large number of linear or cyclic peptidic and peptidomimetic ligands have been developed, which are all related to the common recognition motif RGD[14] and a few potent ligands are presently in different stages of clinical trials for cancer therapy. Notwithstanding these recent achievements, the discovery of new ligands displaying high activity and selectivity together with an optimal pharmacological profile still remains a challenge. Moreover, a clear-cut explanation of the geometrical requirements of the RGD peptidomimetics in their interaction with the different integrins is still lacking (the above-mentioned X-ray structural information suffers from a rather coarse resolution).[5]

New bifunctional diketopiperazine (DKP) scaffolds [**DKP-1** (*cis*) and **DKP-2** (*trans*); Figure 2] were recently developed, which are formally derived from aspartic acid and 2,3-diaminopropionic acid and bear a carboxylic acid and an amino functionality.[15] These bifunctional diketopiperazines were introduced into the 17-membered cyclic RGD peptidomimetics cyclo-[**DKP-1**-RGD] (**9**) and cyclo-[**DKP-2**-RGD] (**10**; Figure 3), and their conformations and biological activities were investigated.[16] Cyclo-[**DKP-2**-RGD] (**10**) effectively inhibited biotinylated vitronectin binding to the purified $\alpha_v\beta_3$ receptor at low nanomolar concentration, whereas cyclo-[**DKP-1**-RGD] (**9**) required a micromolar concentration.[16] These results were interpreted in terms of a more extended RGD sequence imparted by the *trans* geometry of the diketopiperazine scaffold (**DKP-2**) to give rise to a better pre-organization of peptidomimetic **10** for binding to the integrin receptors. These observations prompted us to investigate the structural elements of the bifunctional diketopiperazine scaffold that are able to influence and possibly improve the binding of the cyclo-[DKP-RGD] peptidomimetics.

Herein we present a full account of our investigations and report: 1) the synthesis of a number of cyclic RGD peptidomimetics containing various diketopiperazine scaffolds with different stereochemistry and substitution at the piperazinic nitrogen atoms; 2) the ability of the cyclic RGD peptidomimetics to compete with biotinylated vitronectin for binding to the purified $\alpha_v\beta_3$ and $\alpha_v\beta_5$ receptors; 3) conformational studies of the cyclic RGD peptidomimetics in aqueous solution by ^{1}H NMR spectroscopy experiments; 4) conformational studies of the cyclic RGD peptidomimetics by Monte Carlo/Stochastic Dynamics (MC/SD) simulations; 5) docking studies of the cyclic RGD peptidomimetics in the crystal structure of the $\alpha_v\beta_3$ binding site.

Results and Discussion

Synthesis of the diketopiperazine scaffolds and cyclic RGD peptidomimetics: A collection of eight diketopiperazines

 © 2012 Wiley-VCH Verlag GmbH & Co. KGaA, Weinheim

(**DKP-1**–**DKP-8**) was synthesized, and their stereochemistry and substitution patterns were varied (Figure 2). In particular the scaffolds differ in: 1) the relative stereochemistry, namely *cis* (**DKP-1**) or *trans* (**DKP-2**–**DKP-8**); 2) the absolute stereochemistry of the *trans* scaffolds [3*R*,6*S* (**DKP-2**, **DKP-4**, **DKP-5**) or 3*S*,6*R* (**DKP-3**, **DKP-6**, **DKP-7**, **DKP-8**)]; 3) the substitution at the endocyclic nitrogen atoms, which can be either hydrogen or benzyl (**DKP-2**, **DKP-3**, **DKP-4**, **DKP-6**, **DKP-8**) or dibenzyl (**DKP-5**, **DKP-7**); 4) the length of the side-arm bearing the carboxylic group, which can be either carboxymethyl (**DKP-1**–**DKP-7**) or carboxyethyl (**DKP-8**).

Two different strategies were devised for the synthesis of **DKP-1**–**DKP-8**, depending on their nitrogen substitution. In particular, **DKP-1**, **DKP-2** and **DKP-3** (bearing a benzyl group at nitrogen N-4, Figure 2) were prepared by making use of the serine ligation strategy exemplified in Scheme 1,[17] starting from either (*R*)- or (*S*)-*N*-(*tert*-butoxycarbonyl)aspartic acid β-allyl ester **11**[18] or (*R*)- or (*S*)-*N*-benzylserine methyl ester **12**.[19] Direct coupling of these fragments (HATU, iPr$_2$NEt or EDC, DMAP) led to the isopeptides **14** in high yield, rather than forming the expected dipeptides **13**. As a matter of fact, selective *O*-acylation of the unprotected β-hydroxyl group of *N*-benzylserine methyl ester is preferred to the formation of the tertiary amide and the resulting ester bond is stable in solution to *O*,*N*-acyl transfer.[17] The *O*,*N*-acyl migration was then triggered by cleavage of the Boc protecting group and treatment with a base, which also promoted the simultaneous cyclization to the diketopiperazine **15**. The introduction of the nitrogen functionality was then realized through a Mitsunobu-type reaction by using HN_3·Tol in a toluene/dichloromethane solution, to obtain azide **16** in a moderate (51%; *cis*: *S*,*S*) to good yield (80%; *trans*: *S*,*R* or *R*,*S*).[20] Finally, a one-pot Staudinger reduction/Boc protection[21] yielded the DKP scaffold allyl ester **17**, which was de-allylated[22] to give the amino acid derivatives **DKP-1**, **DKP-2** and **DKP-3** in a quantitative yield.

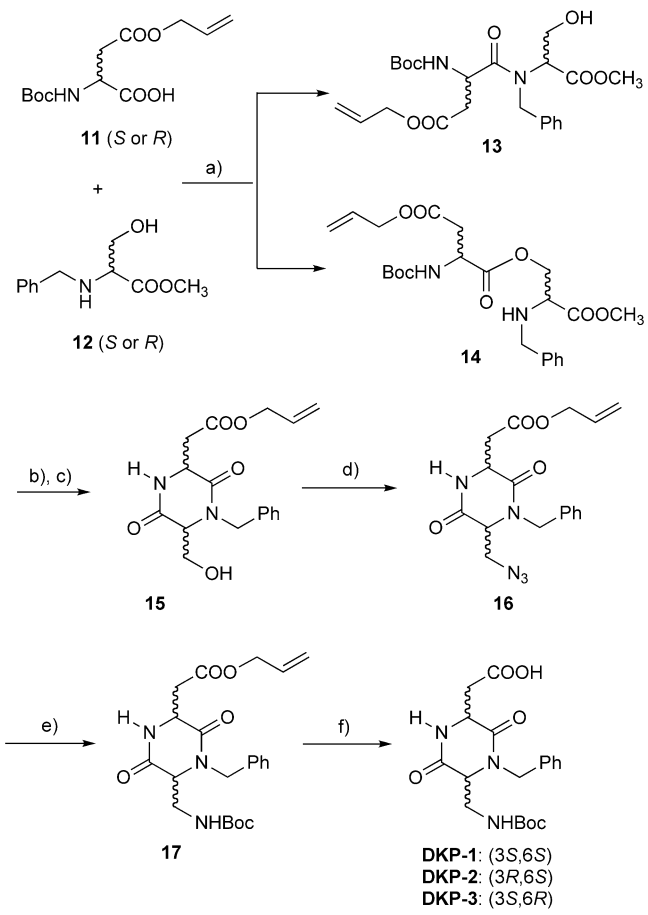

Scheme 1. Synthesis of **DKP-1**, **DKP-2** and **DKP-3** by the serine ligation strategy. a) EDC·HCl, DMAP, CH_2Cl_2, 94%; b) TFA/CH_2Cl_2 1:2; c) DIPEA, iPrOH, 90% over two steps; d) HN_3, DIAD, PPh_3, CH_2Cl_2/toluene, 51% *S*,*S*; 80% *S*,*R* or *R*,*S*; e) Me_3P, BocON, THF, 76%; f) pyrrolidine, PPh_3, $[Pd(PPh_3)_4]$, CH_2Cl_2, 99%.

Scaffold **DKP-8**, bearing a carboxyethyl side chain, was obtained through a similar synthesis strategy starting from (*S*)-*N*-benzylserine methyl ester **12** and (*R*)-*N*-(*tert*-butoxycarbonyl)glutamic acid γ-methyl ester **18** (Scheme 2).[23] Also in this case, direct coupling of the fragments afforded the isopeptide **19**, which was deprotected and cyclized to the diketopiperazine **20**. Azidation of the $-CH_2OH$ group through a Mitsunobu reaction, reduction by catalytic hydrogenation, protection with Boc_2O and final hydrolysis of the methylester afforded **DKP-8**.

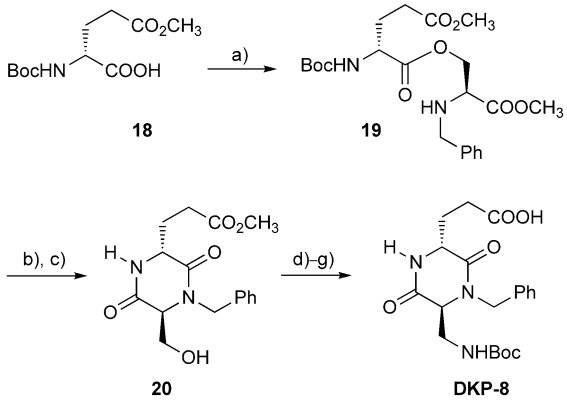

Scheme 2. Synthesis of **DKP-8**: a) **12**, EDC·HCl, DMAP, CH_2Cl_2, 59%; b) TFA/CH_2Cl_2 1:2; c) DIPEA, iPrOH, 93% over two steps; d) HN_3, DIAD, PPh_3, CH_2Cl_2/toluene/DMF; e) H_2, Pd/C, THF; f) Boc_2O, THF; g) LiOH, THF/H_2O_2 1:1, 43% over four steps.

For the preparation of diketopiperazines **DKP-4** and **DKP-6** (bearing a benzyl group at nitrogen N-1, Figure 2), the coupling of Boc-serine to *N*-benzyl-aspartic acid dimethylester **21**[24] was envisaged (Scheme 3). The serine hydroxyl group required protection to avoid self-condensation, and the commercially available Boc-serine *tert*-butyl ether was initially treated with *N*-Bn-Asp dimethyl ester **21** by using several coupling agents: with HATU,[25] PyBrOP[26] and DPPA[27] no product was detected; use of the acyl fluoride, [obtained by treatment of Boc-Ser(O*t*Bu) with cyanuric

 © 2012 Wiley-VCH Verlag GmbH & Co. KGaA, Weinheim

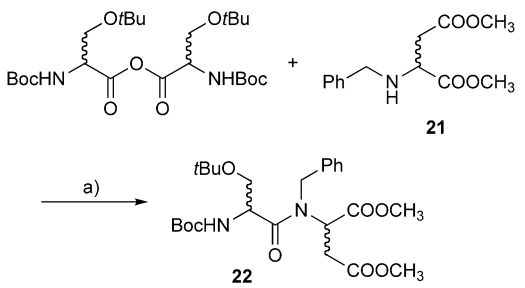

Scheme 3. Synthesis of dipeptide **22**: a) CH_2Cl_2, 80%.

fluoride] afforded the coupling product in a modest 15% yield, whereas use of the mixed anhydride [obtained by treatment of Boc-Ser(O*t*Bu) with *i*BuOCOCl] gave the corresponding iso-butyl carbamate. Finally, preformation of the symmetric Boc-Ser(O*t*Bu) anhydride (DCC)[28] and coupling to *N*-Bn-Asp dimethyl ester **21** afforded the corresponding dipeptide **22** in a satisfactory 80% yield (Scheme 3).

In order to simplify the synthesis sequence and avoid the use of an additional protecting group (*t*Bu), the hydroxyl group of Boc-Ser-OMe (either L or D)[20a] was directly transformed into the corresponding azide under Mitsunobu conditions in 78% yield (Scheme 4).

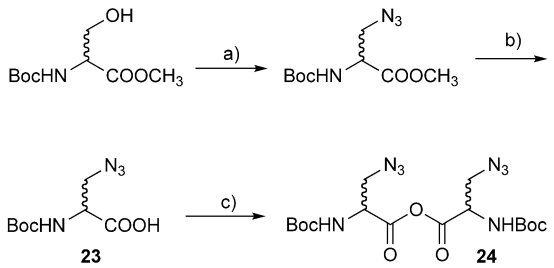

Scheme 4. Synthesis of symmetric anhydride **24**: a) HN_3, DIAD, PPh_3, THF, 78%; b) LiOH, THF/H_2O 1:1, quantitative; c) DCC, CH_2Cl_2, quantitative.

The resulting product was then saponified with LiOH and the freshly prepared acid **23** was treated with DCC to give the symmetric anhydride **24** in a quantitative yield, which was isolated by filtering off DCU and solvent evaporation, and was immediately used in the next synthesis step without further purification. Coupling of 3-azido-2-*N*-*tert*-butoxycarbonylaminopropionic anhydride (**24**) to *N*-benzyl-aspartic acid dimethylester (**21**) occurred in 80% yield, whereas the subsequent Boc cleavage and cyclization to diketopiperazine **26** were nearly quantitative (Scheme 5).

At this stage, diketopiperazine **26** was split in two portions. One portion was subjected to catalytic hydrogenation of the azide, Boc protection and final hydrolysis of the methyl ester to afford diketopiperazines **DKP-4** and **DKP-6** in 90% overall yield (Scheme 6).

A second portion of diketopiperazine **26** was alkylated at nitrogen N-4 (benzyl bromide, KHMDS) to afford the corresponding bis-benzylated derivative. One-pot Staudinger reduction/Boc protection[21] followed by saponification of the methyl ester afforded **DKP-5** and **DKP-7** in 75% overall yield (Scheme 7).

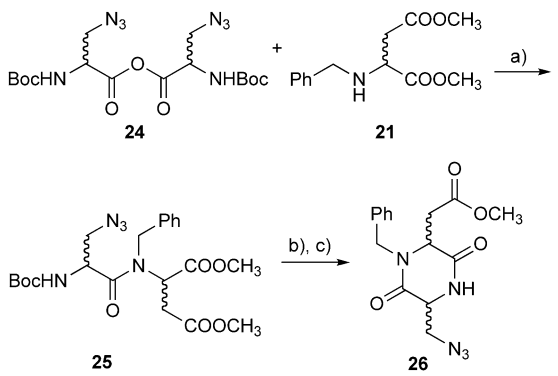

Scheme 5. Synthesis of diketopiperazine **26**: a) CH_2Cl_2, 80%; b) TFA/CH_2Cl_2 1:2; c) DIPEA, *i*PrOH, 90% over two steps.

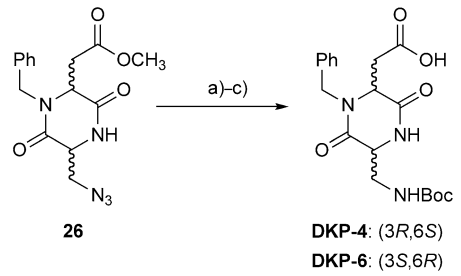

Scheme 6. Synthesis of **DKP-4** and **DKP-6**: a) H_2, Pd/C, THF; b) Boc_2O, THF; c) LiOH, THF/H_2O 1:1, 90% over three steps.

Diketopiperazines **DKP-1**–**DKP-8** were then incorporated into the cyclic RGD derivatives **9**, **10** and **27**–**32** (Figure 4). A solution phase synthesis strategy was adopted, by using Boc-Arg(Mtr), Gly-OBn and Cbz-Asp(O*t*Bu)-OH. The dipeptide Boc-Arg(Mtr)-Gly-OBn was Boc-deprotected and coupled to the acid of the appropriate diketopiperazine scaffold. Subsequent Boc deprotection of the DKP amino group and coupling of the aspartic derivative Cbz-Asp(O*t*Bu)-OH afforded the linear peptidomimetic Cbz-Asp(O*t*Bu)-DKP-Arg(Mtr)-Gly-OBn, which was deprotected by hydrogenolysis (Cbz and Bn) and was subjected to macrolactamization (for detailed conditions, see the Supporting Information).

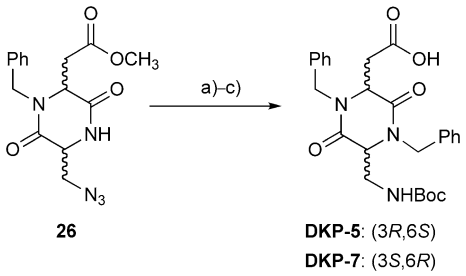

Scheme 7. Synthesis of **DKP-5** and **DKP-7**: a) KHMDS, BnBr, THF/DMF 7:3; b) Me_3P, BocON, THF; c) LiOH, THF/H_2O 1:1, 75% over four steps.

 © 2012 Wiley-VCH Verlag GmbH & Co. KGaA, Weinheim

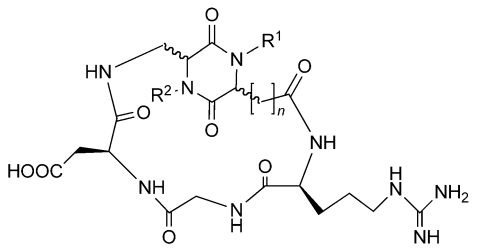

9 = cyclo-(**DKP-1**-RGD) = 3*S*, 6*S*, R^1 = H, R^2 = CH_2Ph, *n* = 1
10 = cyclo-(**DKP-2**-RGD) = 3*R*, 6*S*, R^1 = H, R^2 = CH_2Ph, *n* = 1
27 = cyclo-(**DKP-3**-RGD) = 3*S*, 6*R*, R^1 = H, R^2 = CH_2Ph, *n* = 1
28 = cyclo-(**DKP-4**-RGD) = 3*R*, 6*S*, R^1 = CH_2Ph, R^2 = H, *n* = 1
29 = cyclo-(**DKP-5**-RGD) = 3*R*, 6*S*, R^1 = CH_2Ph, R^2 = CH_2Ph, *n* = 1
30 = cyclo-(**DKP-6**-RGD) = 3*S*, 6*R*, R^1 = CH_2Ph, R^2 = H, *n* = 1
31 = cyclo-(**DKP-7**-RGD) = 3*S*, 6*R*, R^1 = CH_2Ph, R^2 = CH_2Ph, *n* = 1
32 = cyclo-(**DKP-8**-RGD) = 3*S*, 6*R*, R^1 = H, R^2 = CH_2Ph, *n* = 2

Figure 4. Cyclic RGD peptidomimetics containing bifunctional DKP scaffolds.

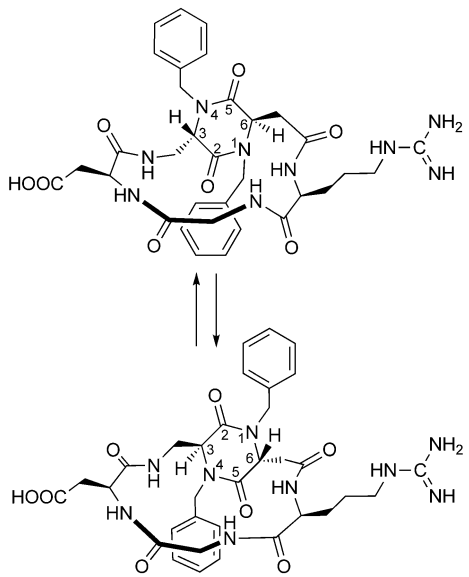

Figure 5. Compounds **31 A** and **31 B**, diastereomers of **31** due to hindered rotation.

Several methodologies were screened for the ring closure, and the best yields were obtained for all the products (except **27**) by using HATU/HOAT as coupling agents in a 1:4:4:6 substrate/HATU/HOAT/iPr_2NEt molar ratio and a substrate concentration of 1.4 mM in DMF.[11b] In the case of cyclo-[**DKP-3**-RGD] (**27**) the highest yield (75%) was obtained by using a 1:3:6 substrate/DPPA/iPr_2NEt molar ratio with the same substrate concentration (1.4 mM) in DMF.[29] A final side-chain deprotection (TFA/thioanisole/ethanedithiol/anisole 90:5:3:2) and preparative HPLC purification afforded the desired compounds **9**, **10** and **27–32** for the biological screening.

In the case of the *N*-dibenzyl derivatives **29** and **31**, the molecules can exist as two different separable conformers (diastereomers) due to hindered rotation of one ring around the other, in a way reminiscent of the *ansa*-cyclopeptides[30] (i.e., the DKP *N*-benzyl group cannot pass inside the macrolactam ring).

With **29**, we were able to isolate only one diastereomer, either because it was formed exclusively or because it was formed predominantly and the minor one was not detected/isolated. With **31**, two diastereomers were isolated in a 2(A):1(B) ratio (Figure 5). The two diastereomers were formed in the macrolactamization step, as shown by the two sets of peaks (2:1 ratio) in the ^{1}H NMR spectrum (see the Supporting Information), but co-eluted in the HPLC. However, after side-chain deprotection, the two diastereomers could be separated, analyzed and subjected to the binding assays (vide infra).

Integrin receptor competitive binding assays: The cyclic RGD peptidomimetics were examined in vitro for their ability to inhibit biotinylated vitronectin binding to the purified $\alpha_v\beta_3$ and $\alpha_v\beta_5$ receptors (Table 1).

Table 1. Inhibition of biotinylated vitronectin binding to $\alpha_v\beta_3$ and $\alpha_v\beta_5$ receptors.

Ligand	Structure	$\alpha_v\beta_3$ IC_{50} [nM][a]	$\alpha_v\beta_5$ IC_{50} [nM][a]
9	cyclo-[**DKP-1**-RGD]	3898 ± 418	> 10^4
10	cyclo-[**DKP-2**-RGD]	3.2 ± 2.7	114 ± 99
27	cyclo-[**DKP-3**-RGD]	4.5 ± 1.1	149 ± 25
28	cyclo-[**DKP-4**-RGD]	7.6 ± 4.3	216 ± 5
29	cyclo-[**DKP-5**-RGD]	12.2 ± 5.0	131 ± 29
30	cyclo-[**DKP-6**-RGD]	2.1 ± 0.6	79 ± 3
31 A	cyclo-[**DKP-7**-RGD]-A	220.2 ± 82.3	> 10^4
31 B	cyclo-[**DKP-7**-RGD]-B	0.2 ± 0.09	109 ± 15
32	cyclo-[**DKP-8**-RGD]	17.7 ± 0.1	420 ± 37
cyclo-[RGDfV]	cyclo-[RGDfV]	3.2 ± 1.3	7.5 ± 4.8
ST1646	see Figure 1	1.0 ± 0.5	1.4 ± 0.8

[a] IC_{50} values were calculated as the concentration of compound required for 50% inhibition of biotinylated vitronectin binding as estimated by GraphPad Prism software; all values are the arithmetic mean ± SD of triplicate determinations.

Screening assays were performed by incubating the immobilized integrin receptors with various concentrations (10^{-12}–10^{-5} M) of the RGD ligands **9**, **10**, **27–32** in the presence of biotinylated vitronectin (1 μg mL^{-1}), and measuring the concentration of bound vitronectin in the presence of the competitive ligands. The ability of the new compounds to inhibit the binding of vitronectin to the isolated $\alpha_v\beta_3$ and $\alpha_v\beta_5$ receptors was compared with that of the reference compounds c(RGDfV)[31] and ST1646[11] (Figure 1). The results are collected in Table 1. Low nanomolar values were obtained with all the ligands except cyclo-[**DKP-1**-RGD] (**9**), which incorporates a *cis* DKP, and ligand **31 A**. The behavior of this last ligand is peculiar, considering that the diastereomeric compound **31 B** (see above for the definition of the two diastereomers) is the most potent ligand of this series, and it effectively inhibits the binding of vitronectin to the isolated $\alpha_v\beta_3$ receptor in subnanomolar concentration. Interestingly, unlike reference compounds c(RGDfV) and ST1646, the

 © 2012 Wiley-VCH Verlag GmbH & Co. KGaA, Weinheim

RGD peptidomimetics **10** and **27–32** were about 10–500-fold more selective for the $\alpha_v\beta_3$ integrin with respect to the $\alpha_v\beta_5$ in this kind of assay.

NMR spectroscopy characterization and conformational studies: The structure and connectivity of ligands **9**, **10** and **27–32** and of their fully protected precursors were unambiguously assigned by means of mono- and bidimensional ^{1}H- and ^{13}C NMR spectroscopy.

The preferred conformations of the cyclic RGD peptidomimetics **9**, **10** and **27–32** in aqueous solution were then investigated, with the aim of rationalizing the affinity of these compounds for the $\alpha_v\beta_3$ receptor at a molecular level. Monodimensional ^{1}H NMR spectroscopy experiments were conducted to detect intramolecular hydrogen bonds, by measuring the chemical shift of the N–H protons and their temperature coefficients ($\Delta\delta/\Delta T$). NOESY spectra were recorded to investigate both sequential and long-range NOEs that provide evidence for preferred conformations. The relevant NMR spectroscopy data are summarized in Table 2.

As already mentioned in our preliminary studies,[16] low affinity ligand **9** exists as an equilibrium of two different preferred conformations. The NOESY spectrum shows two mutually exclusive long-range NOE contacts. The cross-peak between DKP-NH_{10} and NH_{Asp} (strong) is indicative of a β-turn conformation at Gly-Asp stabilized by a hydrogen bond between DKP-NH_{10} and Arg-C=O (referred to as type I H-bonding pattern, Figure 6A). The chemical shift value ($\delta = 7.46$ ppm) and the $\Delta\delta/\Delta T$ value (-2 ppb K^{-1}) of the amide proton DKP-NH_{10} indicate that this proton is strongly locked in an intramolecularly H-bonded state. The cross-peak between NH_{Gly} and NH_{Asp} (medium) is indicative of an alternative β-turn conformation at Arg-Gly, stabilized by a hydrogen bond between Asp-NH and C(8)=O (referred to as type II H-bonding pattern, Figure 6B).

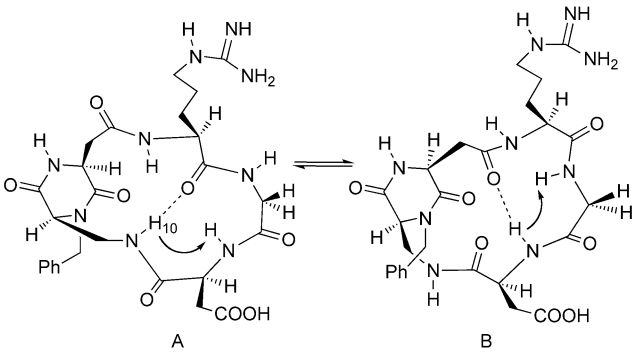

Figure 6. Preferred intramolecular hydrogen-bonded patterns proposed for compound **9** on the basis of spectroscopic data. The arrows indicate significant NOE contacts. A) Type I H-bonding pattern, Gly-Asp β-turn motif. B) Type II H-bonding pattern, Arg-Gly β-turn motif.

High affinity ligands **10** and **27** are apparently characterized by conformational mobility, as suggested by the values of chemical shifts and $\Delta\delta/\Delta T$ reported in Table 2. The only exception is proton NH-Asp of **27** ($\delta = 7.85$ ppm, $\Delta\delta/\Delta T = -3.5$ ppb K^{-1}), which might be involved in a type II H-bonding pattern (for definition of type II H-bonding pattern see Figure 6B). On the other hand, the presence in both cases of a NOE contact between NH_{Gly} and NH_{Arg} suggests the formation of a β-turn motif at DKP-Arg, stabilized by a hydrogen bond between NH_{Gly} and C(5)=O (referred to as type III H-bonding pattern, Figure 7). The presence of this H bond is also supported by the rather upfield chemical shift value of NH_{Gly} in these two ligands ($\delta = 8.18$ and 8.00 ppm for **10** and **27**, respectively) and the relatively low temperature dependence (-5.7 and -4.5 ppb K^{-1}, respectively). The similarity of the NMR spectroscopy data and, hence, of the conformation of these two ligands is quite surprising, considering the opposite configuration of the diketo-

Table 2. ^{1}H NMR spectroscopy and NOE data of cyclic RGD peptidomimetics in water.

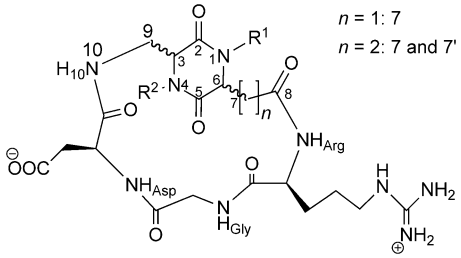

Lig-and	Structure	δ [ppm] NH_1	NH_4	NH_{10}	NH_{Arg}	NH_{Gly}	NH_{Asp}	Δδ/ΔT [ppb K^{-1}] NH_1	NH_4	NH_{10}	NH_{Arg}	NH_{Gly}	NH_{Asp}	Significant NOE contacts
9	cyclo-[**DKP-1**-RGD]	8.35	–	7.46	8.40	8.75	8.10	−7.3	–	−2.0	−7.0	−8.0	−3.7	NH_{Asp}–NH_{10}; NH_{Asp}–NH_{Gly}
10	cyclo-[**DKP-2**-RGD]	8.35	–	8.78	8.57	8.18	8.29	−8.7	–	−10.7	−7.0	−5.7	−7.7	NH_{Arg}–NH_{Gly}
27	cyclo-[**DKP-3**-RGD]	8.10	–	8.28	8.80	8.00	7.85	−5.7	–	−8.5	−6.0	−4.5	−3.5	NH_{Arg}–NH_{Gly}
28	cyclo-[**DKP-4**-RGD]	–	8.17	7.59	8.29	8.27	8.88	–	−9.1	−0.7	−9.3	−8.2	−9.3	–
29	cyclo-[**DKP-5**-RGD]	–	–	8.58	8.48	8.23	8.42	–	–	−11.0	−7.5	−4.7	−8.2	NH_{Arg}–NH_{Gly}
30	cyclo-[**DKP-6**-RGD]	–	8.07	7.90	8.32	8.35	8.80	–	−4.9	−5.1	−7.6	−6.7	−8.0	NH_{Asp}–NH_{10}; NH_4–NH_{10}
31A	cyclo-[**DKP-7**-RGD]-A	–	–	8.04	8.66	7.93	7.76	–	–	−7.5	−5.0	−3.0	−1.0	NH_{Arg}–NH_{Gly}; NH_{Asp}–NH_{Gly}
31B	cyclo-[**DKP-7**-RGD]-B	–	–	7.72	8.34	8.45	8.55	–	–	−4.0	−7.0	−7.0	−5.0	NH_{Asp}–NH_{10}
32	cyclo-[**DKP-8**-RGD]	7.75	–	8.16	8.42	8.27	8.14	−5.3	–	−8.5	−7.2	−6.2	−5.0	NH_1–NH_{Arg}

© 2012 Wiley-VCH Verlag GmbH & Co. KGaA, Weinheim

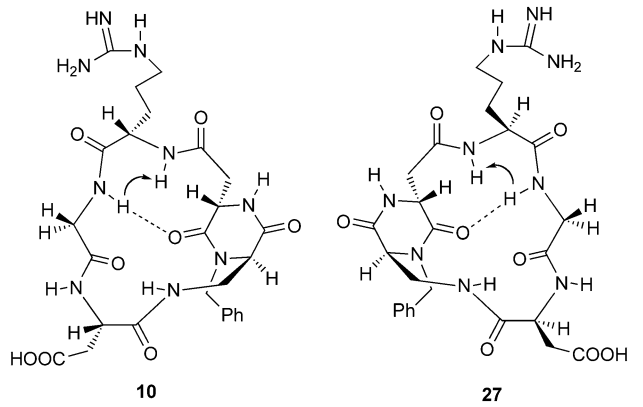

Figure 7. Preferred intramolecular hydrogen-bonded pattern proposed for compound **10** and **27** on the basis of spectroscopic data. The arrows indicate significant NOE contacts. The DKP-Arg β-turn motif is referred to as type III H-bonding pattern.

piperazine scaffold [**DKP-2** (3*R*,6*S*) in **10**; **DKP-3** (3*S*,6*R*) in **27**], which should impart a different stereochemical orientation to the two side arms of the diketopiperazine. This conformational similarity can be interpreted in terms of a quasi-enantiomeric structure of the two ligands (excluding the configuration of the remote RD amino acid side chains, Figure 7).

High affinity ligands **28** and **30**, featuring the diketopiperazine scaffolds **DKP-4** (3*R*,6*S*) and **DKP-6** (3*S*,6*R*), respectively (with the benzyl substitution at the endocyclic nitrogen N-1, instead of N-4), show a different NMR pattern.

In particular, ligand **30** is characterized by a rather strong NOE contact between NH_{Asp} and NH_{10} and a moderate one involving NH_4 and NH_{10}. These two contacts are mutually exclusive and are hence indicative of an equilibrium between two different conformations, respectively, type I and type IV binding modes (Figure 8 A and B). The hydrogen bonded status of the two amide protons NH_4 and NH_{10}, as indicated by their rather low temperature dependence (−4.9 and −5.1 ppb K^{-1}, respectively) and quite upfield chemical shift values ($\delta = 8.07$ and 7.90 ppm, respectively) corroborate

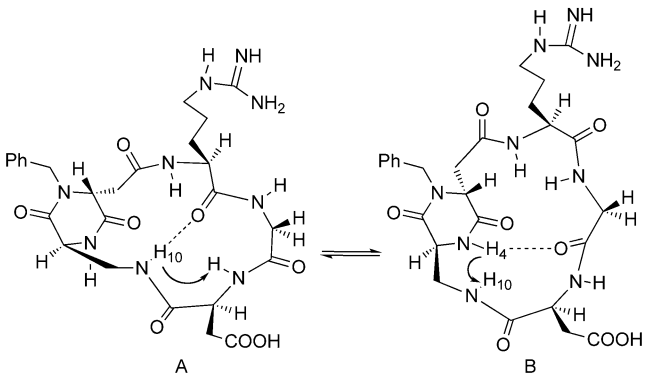

Figure 8. Preferred intramolecular hydrogen-bonded pattern proposed for compound **30** on the basis of spectroscopic data. A) Type I H-bonding pattern, Gly-Asp β-turn motif. B) Type IV H-bonding pattern, pseudo-β-turn at Asp-DKP. The arrows indicate significant NOE contacts.

this assumption. The type IV H-bonding pattern could feature a pseudo-β-turn at Asp-DKP stabilized by a hydrogen bond between NH_4 and Gly-C=O (NOE contact between NH_4 and NH_{10}).

Ligand **28**, on the other hand, is characterized by the absence of relevant NOE contacts, a very low temperature dependence (−0.7 ppb K^{-1}) and a quite upfield chemical shift value ($\delta = 7.59$ ppm) for proton NH_{10}. These two features suggest a type I H-bonding pattern (for definition of type I H-bonding pattern, Figure 6 A or 8 A), notwithstanding the apparent lack of NOE contact between NH_{Asp} and NH_{10}.

The dibenzylated diketopiperazine containing peptidomimetics **29** and **31** were eventually studied. Ligand **29** shows NMR spectroscopy features similar to ligand **10** (for definition of type III H-bonding pattern, see Figure 7): a NOE contact between NH_{Gly} and NH_{Arg} and a rather shielded NH_{Gly} ($\delta = 8.23$ ppm) with a relatively low temperature coefficient (−4.7 ppb K^{-1}). As discussed in the synthesis section, ligand cyclo-[**DKP-7**-RGD] was obtained as a mixture of two diastereomers **31 A** and **31 B**, the conformations of which in solution were studied separately. In particular, the low affinity ligand **31 A** displayed two mutually exclusive NOE contacts between NH_{Arg} and NH_{Gly} and between NH_{Asp} and NH_{Gly}. These three protons, on the other hand, show also a rather strong hydrogen bonded status, as indicated by their low temperature dependence and, at least for NH_{Asp} and NH_{Gly}, their upfield chemical shift (Table 2). These data indicate an equilibrium between two different conformations: one displaying a type III H-bonding pattern (β-turn at DKP-Arg, Figure 7) and a second one showing a type II H-bonding pattern (β-turn at Arg-Gly, Figure 6 B), like the low-affinity ligand **9**, that is, cyclo-[**DKP-1**-RGD]. Finally, high affinity ligand **31 B** shows a single NOE contact between NH_{Asp} and NH_{10} and a hydrogen bonded status for NH_{10} ($\delta = 7.72$ ppm and $\Delta\delta/\Delta T = -4$ ppb K^{-1}, Table 2). These values are indicative of a type I H-bonding pattern (Figure 6 A or 8 A).

Compound **32**, containing the carboxyethyl diketopiperazine scaffold **DKP-8**, is characterized by temperature coefficients of amide protons (Table 2) greater than 5 ppb K^{-1}; this suggests an equilibrium between different conformations. The NOESY spectrum of this ligand shows a strong long-range NOE contact that involves DKP-NH_1 and NH_{Arg} (Figure 9). This contact is indicative of a conformation stabilized by a hydrogen bond between NH_1 and Arg−C=O (referred to as type V H-bonding pattern). The involvement of NH_1 in a hydrogen bond is also confirmed by its relatively low chemical shift value ($\delta = 7.75$ ppm).

Computational studies

Conformational analysis: Conformational studies of the cyclic RGD peptidomimetics were performed by mixed-mode Metropolis Monte Carlo/Stochastic Dynamics (MC/SD) simulations,[32] by using the implicit water GB/SA solvation model[33] and the OPLS_2001 force field.[34,35] As outlined in the Introduction, a key parameter for the RGD fit-

 © 2012 Wiley-VCH Verlag GmbH & Co. KGaA, Weinheim

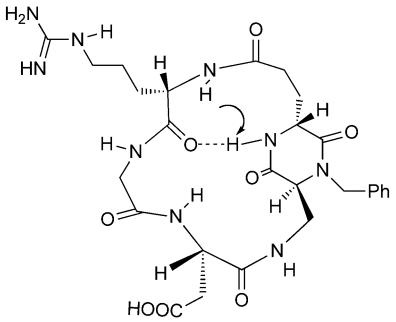

Figure 9. Preferred intramolecular hydrogen-bonded pattern (type V H-bonding pattern) proposed for compound **32** on the basis of spectroscopic data. The arrows indicate significant NOE contacts.

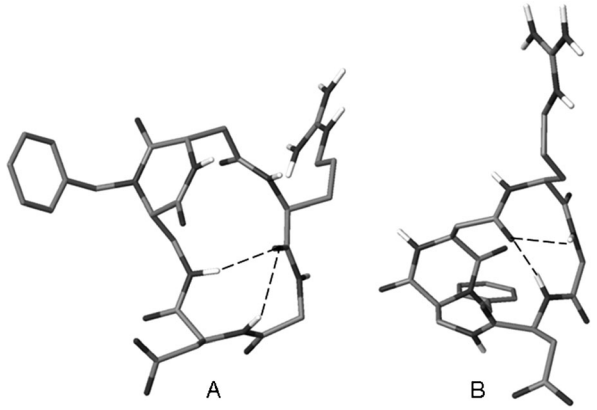

Figure 10. Structures of **9** as obtained by restrained MC/SD simulations based on experimental distance information, after energy minimization. A) Type I-*cis* H-bonding pattern, γ-turn at Gly and βII′-turn at Gly-Asp [Cβ(Arg)−Cβ(Asp) = 7.9 Å]. B) Type II H-bonding pattern, γ-turn at Arg and βII′-turn at Arg-Gly [Cβ(Arg)−Cβ(Asp) = 6.6 Å]. Tube representation: O, N in dark gray, C in light gray and N−H hydrogen atoms in white; for the sake of clarity, all H atoms bound to carbon are omitted.

ting into the active site of the $\alpha_V\beta_3$ integrin is the distance of about 9 Å between the C_β atoms of Asp and Arg, imparted by an extended conformation of the Arg-Gly-Asp sequence.[5] In such an extended conformation, the carboxylate and guanidinium groups are properly positioned to effectively exert their function of electrostatic clamp (vide infra for the relevant docking studies).

As mentioned in our preliminary studies,[16] three-dimensional structures satisfying long-range NOE contacts were generated for low affinity ligand **9** by performing two 10 ns restrained MC/SD simulations and applying the DKP-NH_{10}/NH_{Asp} or the NH_{Asp}/NH_{Gly} distance restraint derived from the NOESY spectra described in the relevant section above. More than 90% of the conformations sampled during the first simulation adopted a non-extended arrangement of the RGD sequence characterized by a β-turn at Gly-Asp and the presence of the corresponding hydrogen bond between DKP-NH_{10} and Arg-C=O. In addition, the formation of a γ-turn at Gly stabilized by the hydrogen bond between NH_{Asp} and Arg-C=O was observed for 40% of the simulation. A Cβ(Arg)−Cβ(Asp) average distance of 7.4 Å was obtained during this MC/SD calculation. A representative energy minimized conformation selected by cluster analysis and featuring both H bonds is shown in Figure 10A (type I-*cis* H-bonding pattern).

Approximately 60% of the conformations sampled during the simulation of **9** featuring the NH_{Asp}/NH_{Gly} distance restraint, adopted a non-extended arrangement of the RGD sequence characterized by a β-turn at Arg-Gly and the corresponding hydrogen bond between NH_{Asp} and C(8)=O. In addition, the formation of a γ-turn at Arg stabilized by the hydrogen bond between NH_{Gly} and C(8)=O was observed for 40% of the simulation. The Cβ(Arg)−Cβ(Asp) average distance in this MC/SD calculation was 6.8 Å. A representative energy minimized conformation selected by cluster analysis and featuring both H bonds is shown in Figure 10B (type II H-bonding pattern).

The NOESY spectra of high affinity ligands **10** (containing *N*-4-benzylated **DKP-2**, 3*R*,6*S*), **27** (containing *N*-4-benzylated **DKP-3**, 3*S*,6*R*) and **29** (containing *N*-dibenzylated **DKP-5** 3*R*,6*S*) showed only one relevant long-range contact between NH_{Gly} and NH_{Arg}: this NOE is indicative of a β-turn motif at DKP-Arg stabilized by a hydrogen bond between NH_{Gly} and C(5)=O (Figure 7, type III H-bonding pattern). The distance restraint corresponding to the NOE contact between NH_{Gly} and NH_{Arg} was applied in the 10 ns MC/SD simulations of compounds **10**, **27** and **29**. More than 90% of the conformations sampled during each of these simulations adopted an extended arrangement of the RGD sequence characterized by a pseudo-β-turn at DKP-Arg and the formation of the corresponding hydrogen bond between the NH_{Gly} and C(5)=O. Interestingly, only for compound **27**, the additional formation of a β-turn at Arg-Gly stabilized by the hydrogen bond between NH_{Asp} and C(8)=O was observed for 15% of the simulations. These results and the NMR spectroscopy data (showing $\delta = 7.85$ ppm and $\Delta\delta/\Delta T = -3.5$ ppb K^{-1} for NH_{Asp} of **27**) suggest the contribution of a type II/type III H-bonding pattern to the conformational equilibrium of **27** (mainly populated by a type III H-bonding pattern). Cβ(Arg)−Cβ(Asp) average distances of 9.3, 8.8, and 9.1 Å were obtained during the MC/SD calculations of **10**, **27** and **29**, respectively. A representative energy minimized conformation selected by cluster analysis and featuring the H bond between the Gly-NH and C(5)=O (type III H-bonding pattern) is shown in Figure 11A for RGD peptidomimetic **10**.

Due to the absence of relevant long-range NOE contacts, several 10 ns runs of unconstrained MC/SD simulations were performed for high affinity ligand **28** (containing *N*-1-benzylated **DKP-4**, 3*R*,6*S*) starting from different 3D structures. Most of the conformations sampled during these simulations adopted an extended arrangement of the RGD sequence [Cβ(Arg)−Cβ(Asp) average distance of 8.8 Å] and approximately 40% of them are characterized by a β-turn at Gly-Asp and the presence of the corresponding hydrogen bond between DKP-NH_{10} and Arg-C=O. These results provide a structural model in agreement with NMR spectroscopy data showing a low temperature dependence

 © 2012 Wiley-VCH Verlag GmbH & Co. KGaA, Weinheim

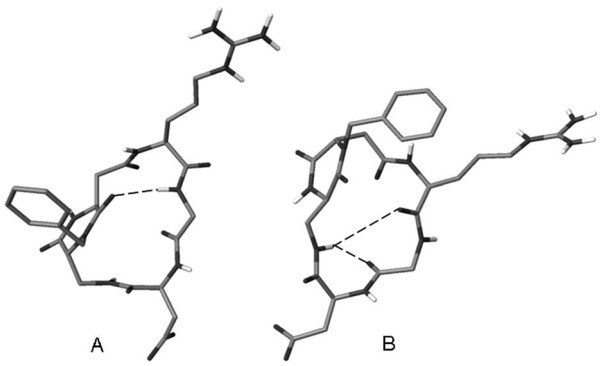

Figure 11. Structures of **10** and **28** as obtained by restrained MC/SD simulations based on experimental distance information, after energy minimization. A) Compound **10**, type III H-bonding pattern, distorted inverse γ-turn at Asp and pseudo-β-turn at DKP-Arg [Cβ(Arg)−Cβ(Asp) = 9.4 Å]. B) Compound **28**, type I-*trans* H-bonding pattern, inverse γ-turn at Asp and distorted βII′-turn at Gly-Asp [Cβ(Arg)−Cβ(Asp) = 9.0 Å]. Tube representation: O, N in dark gray, C in light gray and N−H hydrogen atoms in white; for the sake of clarity, all H atoms bound to carbon are omitted.

(-0.7 ppb K^{-1}) and an upfield chemical shift value ($\delta =$ 7.59 ppm) for proton NH_{10}.

A representative energy minimized conformation selected by cluster analysis and featuring the H bond between DKP-NH_{10} and Arg-C=O (type I-*trans* H-bonding pattern) is shown in Figure 11B for RGD peptidomimetic **28**. It is worth noting how the combination of the *trans* **DKP-4** scaffold with the Gly-Asp β-turn occurs by generating an extended RGD arrangement, whereas the combination of the *cis* **DKP-1** scaffold with the same secondary motif resulted in a non-extended RGD disposition (Figure 10A). Accordingly, two type I H-bonding patterns have been defined (type I-*cis* and type I-*trans*), depending on the *cis* or *trans* relative stereochemistry of the diketopiperazine scaffold.

Three-dimensional structures satisfying long-range NOE contacts were generated for high affinity ligand **30** (containing *N*-1-benzylated **DKP-6**, 3*S*,6*R*) by performing two 10 ns restrained MC/SD simulations and applying the DKP-NH_{10}/NH_{Asp} or the NH_4/NH_{10} distance restraint derived from NOESY spectra (Table 2, Figure 8).

Most of the conformations sampled during the first simulation adopted an extended arrangement of the RGD sequence [Cβ(Arg)−Cβ(Asp) average distance of 9.0 Å] and approximately 40% of them are characterized by a β-turn at Gly-Asp and the corresponding hydrogen bond between DKP-NH_{10} and Arg-C=O. A representative energy minimized conformation selected by cluster analysis and featuring this H bond is shown in Figure 12A (type I-*trans* H bonding pattern). Approximately 70% of the conformations sampled during the simulation of **30** featuring the NH_4/NH_{10} distance restraint adopted an extended arrangement of the RGD sequence [Cβ(Arg)−Cβ(Asp) average distance of 8.8 Å] characterized by a pseudo-β-turn at Asp-DKP and the corresponding hydrogen bond between NH_4 and Gly-C=O. In addition, the formation of a γ-turn at Asp stabilized by the hydrogen bond between NH_{10} and Gly-C=O was observed for 50% of the simulation. A representative energy minimized conformation selected by cluster analysis and featuring these H bonds is shown in Figure 12B (type IV H-bonding pattern).

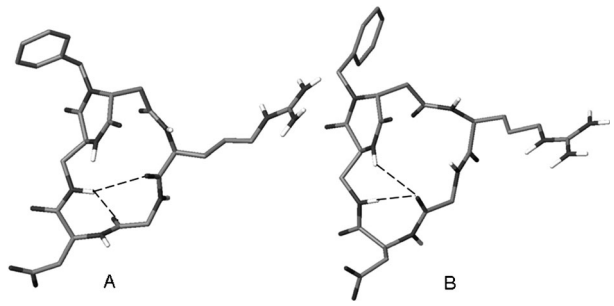

Figure 12. Structures of **30** as obtained by restrained MC/SD simulations based on experimental distance information, after energy minimization. A) Type I-*trans* H-bonding pattern, inverse γ-turn at Asp and distorted βII′-turn at Gly-Asp [Cβ(Arg)−Cβ(Asp) = 9.0 Å]. B) Type IV H-bonding pattern, inverse γ-turn at Asp and pseudo-β-turn at Asp-DKP [Cβ(Arg)−Cβ(Asp) = 8.8 Å]. Tube representation: O, N in dark gray, C in light gray and N−H hydrogen atoms in white; for the sake of clarity, all H atoms bound to carbon are omitted.

Three-dimensional structures satisfying long-range NOE contacts were generated for RGD peptidomimetic **31** (containing *N*-dibenzylated **DKP-7**, 3*S*,6*R*) by performing three 10 ns restrained MC/SD simulations and applying the following distance restraints derived from NOESY spectra of diastereoisomers **31A** and **31B** (Table 2): in the first simulation a NH_{Arg}/NH_{Gly} restraint, relevant in **31A**, in the second simulation a NH_{Asp}/NH_{Gly} restraint, also relevant in **31A**, and in the third simulation a DKP-NH_{10}/NH_{Asp} restraint, relevant in **31B**.

All the conformations sampled during the first two simulations adopted a non-extended arrangement of the RGD sequence [Cβ(Arg)−Cβ(Asp) average distance of 6.6 Å] characterized by the simultaneous presence of different turn motifs (pseudo-β-turn at DKP-Arg, γ-turn at Gly and pseudo-β-turn centered at the DKP unit). The structural models provided by these restrained MC/SD simulations differ from the conformations hypothesized on the basis of NMR spectroscopy data of **31A** [equilibrium between type III (pseudo-β-turn at DKP-Arg) and type II (β-turn at Arg-Gly) H-bonding patterns, see the NMR spectroscopy section]. However, also the calculated structures are able to provide an explanation for the NOE contacts and the NMR temperature coefficients observed for low affinity ligand **31A**.

The distance restraint corresponding to the NOE contact between DKP-NH_{10} and NH_{Asp} (observed in the NOESY spectrum of high affinity ligand **31B**) was applied in the third 10 ns MC/SD simulation of compound **31**. Most of the conformations sampled during this simulation adopted an extended arrangement of the RGD sequence [Cβ(Arg)−Cβ(Asp) average distance of 9.0 Å] and approximately 50% of them are characterized by a β-turn at Gly-Asp and the corresponding hydrogen bond between DKP-NH_{10} and Arg-C=O (type I-*trans* H-bonding pattern).

 © 2012 Wiley-VCH Verlag GmbH & Co. KGaA, Weinheim

Contrary to what was observed for the other cyclic RGD peptidomimetics containing DKP scaffolds, rotation of the DKP ring cannot be observed during the simulations performed on compound **31**; this confirms **31A** and **31B** as two different separable conformers (diastereomers) due to hindered rotation of one ring around the other.

The distance restraint corresponding to the NOE contact between NH_1 and NH_{Arg} was applied in the 10 ns MC/SD simulation of RGD peptidomimetic **32** (containing *N*-4-benzylated **DKP-8**, 3*S*,6*R*). Approximately 60% of the conformations sampled during this simulation adopted an extended arrangement of the RGD sequence characterized by the formation of the hydrogen bond between NH_1 and Arg-C=O (Figure 9, type V H-bonding pattern). In addition, the formation of the hydrogen bond between NH_{Asp} and C(2)=O (type Va H-bonding pattern) or the presence of a β-turn at Gly-Asp stabilized by the hydrogen bond between DKP-NH_{10} and Arg-C=O (type Vb H-bonding pattern) were observed for 35 and 25% of the simulation, respectively.

Representative energy minimized conformations selected by cluster analysis and featuring the type Va and Vb H-bonding patterns are shown in Figure 13 for RGD peptidomimetic **32**.

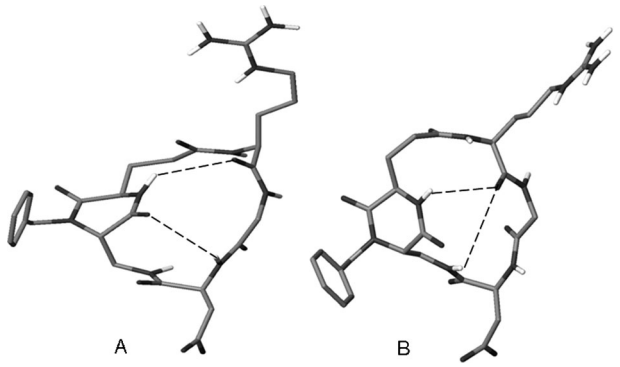

Figure 13. Structures of **32** as obtained by restrained MC/SD simulation based on experimental distance information, after energy minimization. A) Type Va H-bonding pattern [Cβ(Arg)−Cβ(Asp) = 9.9 Å]. B) Type Vb H-bonding pattern [Cβ(Arg)−Cβ(Asp) = 9.1 Å]. Tube representation: O, N in dark gray, C in light gray and N−H hydrogen atoms in white; for the sake of clarity, all H atoms bound to carbon are omitted.

Molecular docking: In order to rationalize, on a molecular basis, the affinity of cyclic RGD peptidomimetics for the $\alpha_v\beta_3$ receptor, docking studies were performed by starting from the representative conformations obtained from the MC/SD simulations. The crystal structure of the extracellular segment of integrin $\alpha_v\beta_3$ complexed with the cyclic pentapeptide Cilengitide (PDB ID: 1L5G) was taken as a reference model for the interpretation of the docking results in terms of ligand–protein interactions.[5] In the X-ray complex, Cilengitide binds to the interface of the α and β units forming specific electrostatic interactions. The acid and basic pharmacophoric groups and their orientation are essential for binding to the $\alpha_v\beta_3$ because they act like an electrostatic clamp, interacting with charged regions of the receptor binding site.

Docking calculations starting from geometries featuring the type I-*cis* and type II H-bonding patterns produced top-ranked binding modes conserving optimal interactions only with the α subunit of the $\alpha_v\beta_3$ receptor. Probably, the short Cβ(Arg)−Cβ(Asp) distances (values lower than 8 Å) of these geometries prevent the guanidine and carboxylic groups from achieving the required separation for binding to the $\alpha_v\beta_3$ integrin. On the other hand, docking calculations starting from the RGD extended conformations featuring the type I-*trans*, type III, type IV and type V H-bonding patterns [Cβ(Arg)−Cβ(Asp) distance values ≥8.8 Å] produced top-ranked binding modes conserving all the important interactions of the X-ray complex. As an example, the best pose obtained for the highest affinity ligand **31B** featuring the type I-*trans* H-bonding pattern is shown in Figure 14.

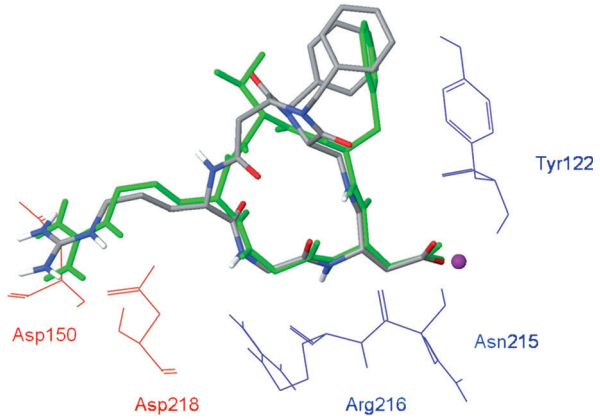

Figure 14. Docking best pose of compound **31B** (type I-*trans* H-bonding pattern, atom color tube representation) into the crystal structure of the extracellular domain of $\alpha_v\beta_3$ integrin (α unit red and β unit blue wire representation) overlaid on the bound conformation of Cilengitide (green tube representation). Only selected integrin residues involved in the interactions with the ligand are shown. The Mn^{2+} ion at MIDAS is shown as a magenta CPK sphere. For the sake of clarity, all H atoms bound to carbon are omitted.

The positively charged Arg guanidinium group of the ligand interacts with the negatively charged side chains of Asp218 and Asp150 in the α unit, one carboxylate oxygen of the ligand Asp side chain is coordinated to the metal cation in the metal-ion-dependent adhesion site (MIDAS) region of the β unit, whereas the second carboxylate oxygen forms hydrogen bonds with the backbone amides of Asn215 and Tyr122 in the β unit. Further stabilizing interaction involves the formation of a hydrogen bond between the ligand backbone NH of the Asp residue and the backbone carbonyl group of Arg216 in the β unit. Favorable aromatic ring interactions between the ligand benzylic groups and the β_3-Tyr122 side chain could also be observed (Figure 14).

In light of all these considerations, the micromolar affinity of RGD peptidomimetics **9** and **31A** (3.9 and 0.2 μM, respectively) for $\alpha_v\beta_3$ (Table 1) can be explained in terms of their

 © 2012 Wiley-VCH Verlag GmbH & Co. KGaA, Weinheim

low pre-organization for binding. In fact, as determined by the computational and NMR spectroscopy studies, in solution these compounds mainly feature non-extended RGD conformations, which according to the docking results, are not able to properly fit into the $\alpha_v\beta_3$ receptor. On the contrary, the nanomolar affinity of RGD peptidomimetics **10**, **27–30**, **31B** and **32** for $\alpha_v\beta_3$ can be attributed to their high structural pre-organization. In fact, as determined by the computational and NMR spectroscopy studies, these compounds in solution mainly feature extended RGD conformations (principally determined by type I-*trans*, type III, type IV and type V H-bonding patterns) similar to the RGD bound conformation of Cilengitide.

Conclusion

In summary, we have synthesized a small library of bifunctional diketopiperazine (DKP) scaffolds, which were formally derived from 2,3-diaminopropionic acid and aspartic acid (**DKP-1**–**DKP-7**) or glutamic acid (**DKP-8**) and feature an amine and a carboxylic acid functional group. The scaffolds differ for the configuration at the two stereocenters and the substitution at the diketopiperazinic nitrogen atoms. The bifunctional diketopiperazines were introduced into eight cyclic peptidomimetics containing the Arg-Gly-Asp (RGD) sequence. The resulting RGD peptidomimetics were screened for their ability to inhibit biotinylated vitronectin binding to the purified integrins $\alpha_v\beta_3$ and $\alpha_v\beta_5$, which are involved in tumor angiogenesis. Nanomolar values were obtained for the RGD peptidomimetics derived from *trans* DKP scaffolds (**DKP-2**–**DKP-8**). Conformational studies of the cyclic RGD peptidomimetics by ^{1}H NMR spectroscopy experiments (VT-NMR and NOESY) in aqueous solution and Monte Carlo/Stochastic Dynamics (MC/SD) simulations revealed that the highest affinity ligands display well-defined preferred conformations featuring intramolecular hydrogen-bonded turn motifs and an extended arrangement of the RGD sequence [Cβ(Arg)−Cβ(Asp) average distance $\geq$8.8 Å]. Docking studies were performed, starting from the representative conformations obtained from the MC/SD simulations and taking as a reference model the crystal structure of the extracellular segment of integrin $\alpha_v\beta_3$ complexed with the cyclic pentapeptide, Cilengitide. The highest affinity ligands produced top-ranked poses conserving all the important interactions of the X-ray complex.

Experimental Section

A detailed procedure for the synthesis of intermediate **15** starting from protected amino acid derivatives **11** and **12** was already reported.[16] The same procedure was used for the synthesis of intermediate **20**, starting from protected amino acid derivatives **18** and **12**. Diketopiperazine **26** ring closure was achieved under similar conditions by using Et_3SiH (2.5 equiv) as a scavenger during Boc cleavage.

General procedure for the synthesis of diketopiperazine azides: PPh_3 (1.5 equiv) was added to a solution of diketopiperazines **15** or **20** (1 equiv) in CH_2Cl_2/toluene (2:1) under a nitrogen atmosphere and at −20 °C, and the mixture was stirred until a solution was obtained. Hydrazoic acid (1.5 M in toluene, 3 equiv) was added followed by dropwise addition of DIAD (1.5 equiv) and the reaction was stirred at −20 °C for 3–16 h. The reaction mixture was loaded onto a silica gel column and purified by flash chromatography (for solvents and ratios used, see the Supporting Information) to afford the desired product as a white foam (69–86 %).

General procedure for the synthesis of dipeptide 25: DCC (1 equiv) was added to a solution of either (*R*)- or (*S*)-*N*-Boc-Ser(N_3)-OH (**23**; 2 equiv) in CH_2Cl_2, in one portion. A white precipitate (DCU) formed and stirring was continued for 1 h at room temperature. The mixture was then filtered on cotton wool to remove DCU. The white DCU residue was washed twice with cold CH_2Cl_2. The filtrate was concentrated under reduced pressure at room temperature, and dried under high vacuum to afford symmetric anhydride **24** as a pale yellow foam, which was used without further purification. Either (*R*)- or (*S*)-*N*-benzyl-aspartic acid dimethylester (0.7 equiv) was dissolved in CH_2Cl_2 and the mixture was cooled to 0 °C. A solution of symmetric anhydride in CH_2Cl_2 was then added dropwise (very slowly). The reaction mixture was allowed to reach room temperature and was stirred at room temperature, overnight. The solvent was then removed under reduced pressure and the residue was purified by flash chromatography (hexane/EtOAc 8:2) on silica gel to afford the desired product as a viscous transparent oil (80 %).

General diketopiperazine *N*-benzylation procedure: A flame-dried flask under N_2 was charged with a solution of **26** (1 equiv) in dry THF. The temperature was lowered to −78 °C and KHMDS (0.5 M solution in toluene, 1.1 equiv) was added dropwise. After 30 min benzyl bromide (5 equiv) was added, and a final solvent ratio THF/DMF 7:3 was reached by adding DMF. The mixture was allowed to reach −40 °C and stirred for 3 h. Then aqueous NH_4Cl was slowly added and the mixture was extracted with EtOAc (3×). The organic phases were then washed with brine and dried over Na_2SO_4. Volatiles were removed under reduced pressure and the residue was purified by flash chromatography on silica gel to afford the desired product as a viscous transparent oil (86 %).

General procedure for diketopiperazine azide reduction and Boc protection: A) 2-(*tert*-Butoxycarbonyloxyimino)-2-phenylacetonitrile (Boc-ON, 2.2 equiv) and Me_3P (1 M solution in toluene, 2 equiv) were added successively to a solution of diketopiperazine azide (1 equiv) in THF, under a nitrogen atmosphere and at −20 °C. After being stirred for 6 h at room temperature, the solution was diluted with CH_2Cl_2 and washed with H_2O (3×) and brine. The organic phase was dried over Na_2SO_4 and volatiles were removed under reduced pressure. The residue was purified by flash chromatography (for solvents and ratios used, see the Supporting Information) on silica gel to afford the desired product as a white foam (76–87 %).

B) Diketopiperazine azide (1 equiv) was dissolved in THF and Pd/C (0.1 equiv) was added. The flask was thoroughly purged with H_2, and the system was closed. The reaction mixture was stirred at room temperature for 4 h, and then filtered through a Celite pad. The cake thus obtained was thoroughly washed with THF. The filtrate was concentrated and dried to give the crude product as a transparent paste (95 %), which was dissolved in THF (35 mL). Boc_2O (1.1 equiv) was then added in one portion. After stirring the mixture at room temperature, overnight, EtOAc was added. The solution was washed with $KHSO_4$ (1 M; 4×) and brine (1×). The organic phase was dried over Na_2SO_4 and volatiles were removed under reduced pressure, to afford the desired product as a white foam (95 %), which was used without further purification.

General procedure for diketopiperazine allyl ester deprotection: Diketopiperazine allyl ester (1 equiv) was dissolved in CH_2Cl_2 under a nitrogen atmosphere. After cooling the solution at 0 °C, pyrrolidine (1.2 equiv), PPh_3 (0.18 equiv) and $[Pd(PPh_3)_4]$ (0.04 equiv) were added successively. After being stirred for 1 h at 0 °C, the mixture was diluted with EtOAc and extracted with aqueous $NaHCO_3$ (4×). The combined aqueous phases were acidified to pH 2 with a $KHSO_4$ (1 M) solution and then extracted with CH_2Cl_2. The resulting organic phase was dried over Na_2SO_4 and the solvent was evaporated to afford the desired product as a fluffy white solid (99 %).

 © 2012 Wiley-VCH Verlag GmbH & Co. KGaA, Weinheim

Procedure for diketopiperazine methyl ester hydrolysis: A) Diketopiperazine methyl ester (1 equiv) was dissolved in THF and the mixture was cooled to 0°C. A solution of $LiOH{\cdot}H_2O$ (2.5 equiv) in H_2O was added dropwise. The resulting solution was stirred for 1 h at 0°C. Then, maintaining the temperature at 0°C, the mixture was acidified with HCl (1 M) to pH 1–2, and extracted with CH_2Cl_2 (4×). The collected organic phases were dried over Na_2SO_4 and volatiles were removed under reduced pressure. Either **DKP-4** or **DKP-6** were afforded as a white foam (100%). B) Diketopiperazine methyl ester (1 equiv) was dissolved in THF. The mixture was cooled to 0°C and a solution of LiOH (2.7 M) in H_2O_2 (35% v/v) was added dropwise. The mixture was stirred for an additional 30 min at 0°C, then warmed to room temperature and stirred for 7 h. After addition of Na_2SO_3 (6 equiv) the reaction mixture was diluted with THF/H_2O (1:1). $KHSO_4$ (1 M) was then added until pH 1–2 was reached, and the mixture was extracted with DCM (4×). The collected organic phases were dried over Na_2SO_4 and volatiles removed under reduced pressure, to afford crude **DKP-8** as a yellowish solid. The crude product was dissolved in EtOAc and extracted with a saturated $NaHCO_3$ aqueous solution; collected aqueous layers were acidified with $KHSO_4$ (1 M) to reach pH 1–2, and extracted with DCM (4×). Collected organic phases were dried over Na_2SO_4 and volatiles were removed under reduced pressure, to afford **DKP-8** as a white foam (90%).

General procedure for Boc deprotection reactions: A half volume of TFA was added to a solution of the *N*-Boc-protected amino acid or peptide in CH_2Cl_2 (0.13 M). The reaction mixture was stirred for 2 h at room temperature and then concentrated at reduced pressure. Excess TFA was azeotropically removed from the residue with toluene. Diethyl ether was added to the residue and the resulting suspension was evaporated under reduced pressure to afford the corresponding TFA salt.

General procedure for coupling reactions: HATU (1.2 equiv), HOAt (1.2 equiv) and DIPEA (4 equiv) were added successively to a solution of the N-protected amino acid in DMF, under a nitrogen atmosphere and at 0°C. After 30 min, a solution of the N-deprotected TFA salt of the peptide in DMF was added and the reaction mixture was stirred at 0°C for 1 h and at room temperature, overnight. The mixture was then diluted with EtOAc and consecutively washed with $KHSO_4$ (1 M; 2×), a saturated $NaHCO_3$ aqueous solution (2×), brine (2×), and dried over Na_2SO_4. Volatiles were evaporated under reduced pressure to afford the crude product.

General procedure for Cbz and OBn hydrogenolytic cleavage: Protected compound (1 equiv) was dissolved in a mixture of THF/H_2O (1:1) and Pd/C 10% (0.1 equiv) was added. The reaction mixtures were subjected to three vacuum/hydrogen cycles and then stirred, overnight, at room temperature under 1 bar of hydrogen. The mixture was filtered through Celite, and the cake thus obtained was washed thoroughly with THF/H_2O (1:1). The filtrate was concentrated and dried to give the crude product as white solid (100%).

General procedure for macrolactamization: HATU (4 equiv), HOAt (4 equiv) and DIPEA (6 equiv) were added successively to a solution of deprotected linear compound (1.4 mM; 1 equiv) in DMF, under a nitrogen atmosphere at 0°C. After stirring the reaction mixture at 0°C for 1 h, it was allowed to reach room temperature and stirred, overnight. DMF was then removed under reduced pressure and the residue was purified by flash chromatography (CH_2Cl_2/MeOH; for ratios used, see the Supporting Information) on silica gel to afford the product as white foam (31–74%).

Solid-phase receptor-binding assay: Purified $\alpha_v\beta_3$ and $\alpha_v\beta_5$ receptors (Chemicon International, Inc., Temecula, CA) were diluted to 0.5 $\mu g\,mL^{-1}$ in coating buffer containing Tris-HCl (20 $mmol\,L^{-1}$; pH 7.4), NaCl (150 $mmol\,L^{-1}$), $MnCl_2$ (1 $mmol\,L^{-1}$), $CaCl_2$ (2 $mmol\,L^{-1}$) and $MgCl_2$ (1 $mmol\,L^{-1}$). An aliquot of diluted receptors (100 μL per well) was added to 96-well microtiter plates (Nunc MW 96F Medisorp Straight) and incubated, overnight, at 4°C. The plates were then incubated with blocking solution (coating buffer plus 1% bovine serum albumin) for an additional 2 h at room temperature to block nonspecific binding followed by 3 h incubation at room temperature with various concentrations (10^{-12}–10^{-5} M) of test compounds in the presence of vitronectine (1 $\mu g\,mL^{-1}$) biotinylated by using EZ-Link Sulfo-NHS-Biotinylation kit (Pierce, Rockford, IL). After washing, the plates were incubated for 1 h at room temperature with streptavidin–biotinylated peroxidase complex (Amersham Biosciences, Uppsala, Sweden) followed by 30 min incubation with substrate reagent solution (100 μL; R&D Systems, Minneapolis, MN) before stopping the reaction by addition of H_2SO_4 (2 N, 50 μL). Absorbance at 415 nm was read in a Synergy™ HT multi-detection microplate reader (BioTek Instruments, Inc.). Each data point is the result of the average of triplicate wells and was analyzed by nonlinear regression analysis with Prism GraphPad program. Each experiment was repeated in triplicate.

General procedure for Mtr and O*t*Bu ester removal: Protected macrolactams were treated with TFA (0.01 M) in the presence of ion scavengers: thioanisole (5%), ethanedithiol (3%), anisole (2%). After TFA removal, under reduced pressure, the residue was dissolved in a 1:1 mixture of diisopropyl ether/water. Phases were separated and the aqueous layer was washed several times with diisopropyl ether. The aqueous phase was concentrated under reduced pressure to give the crude product, which was purified by HPLC to give the desired compound as white solid (60–80%).

NMR spectroscopy studies: NMR spectroscopy experiments were performed at a temperature of 298 K on Bruker Avance 400 and 600 MHz spectrometers. All proton and carbon chemical shifts were assigned unambiguously. The NMR experiments were carried out in a D_2O/H_2O 1:9 mixture in order to observe amide protons. Two-dimensional experiments (TOCSY, NOESY, and HSQC) were carried out on samples of cyclic RGD peptidomimetics **9**, **10**, **27**–**32** at a concentration range of 3–6 mM. NOESY experiments were performed at 0.7 or 0.8 s. The water resonance was saturated with the excitation sculpting sequence from the Bruker library. The conformations of the cyclic pentapeptides were analyzed with respect to hydrogen bonding of amide protons (VT-NMR spectroscopy) and NOE contacts.

Computational studies: All calculations were run by using the Schrödinger suite of programs (http://www.schrodinger.com) through the Maestro graphical interface.

Conformational analysis: Conformational preferences of the RGD peptidomimetics were investigated by Monte Carlo/Stochastic Dynamics (MC/SD) hybrid simulations[32] by using the NMR spectroscopy restraints derived from the experimental NOE contacts (for distance restraints used for each calculation, see the Supporting Information). All the NOE restraints were set to a distance value of 2(±0.5) Å with a force constant of 100 $kJ\,mol^{-1}\,Å^{-2}$. MC/SD simulations were performed at 300 K within the framework of MacroModel version 9.5[36] by employing the OPLS_2001 force field[34] and the implicit water GB/SA solvation model.[33] RGD side-chain dihedral angles were defined as internal coordinate degrees of freedom in the Monte Carlo part of the algorithm. A time step of 1 fs was used for the stochastic dynamics (SD) part of the algorithm for 10 ns of simulation time. Samples were taken at 2 ps intervals during each simulation, yielding 5000 conformations for analysis. The percentages of H bonds discussed here were calculated as percentages of conformations sampled during the simulation in which donor H–acceptor O distance <2.5 Å (γ-turn) or <4 Å (β-turn).

Molecular docking: The recently solved crystal structure of the extracellular domain of the integrin $\alpha_v\beta_3$ receptor in complex with Cilengitide and in the presence of the proadhesive ion Mn^{2+} (PDB ID: 1L5G)[5] was used for docking studies. Docking was performed only on the globular head of the integrin because the headgroup of integrin has been identified in the X-ray structure as the ligand-binding region. The protein structure was setup for docking as follows. The protein was truncated to residue sequences 41–342 for chain α and 114–347 for chain β. Due to a lack of parameters, the Mn^{2+} ions in the experimental protein structure were modeled by replacing them with Ca^{2+} ions. The resulting structure was prepared by using the Protein Preparation Wizard of the graphical user interface Maestro and the OPLSAA force field. The automated docking calculations were performed by using Glide[37] (Grid-based Ligand Docking with Energetics). The grid generation step started from the extracellular fragment of X-ray structure of $\alpha_v\beta_3$ complex with Cilengitide, as described in the protein setup section. The center of the grid enclosing box was defined by the center of the bound ligand, as described

 © 2012 Wiley-VCH Verlag GmbH & Co. KGaA, Weinheim

in the original PDB entry. The enclosing box dimensions, which are automatically deduced from the ligand size, fit the entire active site. For the docking step, the size of the bounding box for placing the ligand center was set to 12 Å. No further modifications were applied to the default settings. The GlideScore function was used to select 20 poses for each ligand. The Glide program was initially tested for its ability to reproduce the crystallized binding geometry of Cilengitide. The program was successful in reproducing the experimentally determined binding mode of this compound, as it corresponds to the best-scored pose.

Acknowledgements

We thank Milan University for PhD Fellowships (to M.M., M.M., R.C. and I.G.). We also gratefully acknowledge Ministero dell'Università e della Ricerca for financial support (PRIN prot. 2008J4YNJY). U.P. thanks Fondazione CARIPLO for a research grant (Project: RedDrugTrain).

[1] R. O. Hynes, *Cell* **2002**, *110*, 673–687.
[2] M. Shimaoka, T. A. Springer, *Nat. Rev. Drug Discovery* **2003**, *2*, 703–716.
[3] P. C. Brooks, A. M. Montgomery, M. Rosenfeld, R. A. Reisfeld, T. Hu, G. Klier, D. A. Cheresh, *Cell* **1994**, *79*, 1157–1164.
[4] E. F. Plow, T. A. Haas, L. Zhang, J. Loftus, J. W. Smith, *J. Biol. Chem.* **2000**, *275*, 21785–21788.
[5] J.-P. Xiong, T. Stehle, R. Zhang, A. Joachimiak, M. Frech, S. L. Goodman, M. A. Arnaout, *Science* **2002**, *296*, 151–155.
[6] M. A. Dechantsreiter, E. Planker, B. Mathä, E. Lohof, G. Hölzemann, A. Jonczyk, S. L. Goodman, H. Kessler, *J. Med. Chem.* **1999**, *42*, 3033–3040.
[7] K.-E. Gottschalk, H. Kessler, *Angew. Chem.* **2002**, *114*, 3919–3927; *Angew. Chem. Int. Ed.* **2002**, *41*, 3767–3774.
[8] C. Mas-Moruno, F. Rechenmacher, H. Kessler, *Anti-Cancer Agents Med. Chem.* **2010**, *10*, 753–768.
[9] L. Auzzas, F. Zanardi, L. Battistini, P. Burreddu, P. Carta, G. Rassu, C. Curti, G. Casiraghi, *Curr. Med. Chem.* **2010**, *17*, 1255–1299.
[10] a) G. Casiraghi, G. Rassu, L. Auzzas, P. Bureddu, E. Gaetani, L. Battistini, F. Zanardi, C. Curti, G. Nicastro, L. Belvisi, I. Motto, M. Castorina, G. Giannini, C. Pisano, *J. Med. Chem.* **2005**, *48*, 7675–7687; b) F. Zanardi, P. Bureddu, G. Rassu, L. Auzzas, L. Battistini, C. Curti, A. Sartori, G. Nicastro, G. Menchi, N. Cini, A. Bottonocetti, S. Raspanti, G. Casiraghi, C. Pisano, *J. Med. Chem.* **2008**, *51*, 1771–1782.
[11] a) L. Belvisi, T. Riccioni, M. Marcellini, I. Chiarucci, D. Efrati, L. Vesci, D. Potenza, C. Scolastico, L. Manzoni, K. Lombardo, M. A. Stasi, B. Nico, D. Ribatti, M. Presta, P. Carminati, C. Pisano, *Mol. Cancer Ther.* **2005**, *4*, 1670–1680; b) L. Belvisi, A. Bernardi, M. Colombo, L. Manzoni, D. Potenza, C. Scolastico, G. Giannini, M. Marcellini, T. Riccioni, M. Castorina, P. LoGiudice, C. Pisano, *Bioorg. Med. Chem.* **2006**, *14*, 169–180; c) L. Manzoni, L. Belvisi, D. Arosio, M. Civera, M. Pilkington-Miksa, D. Potenza, A. Caprini, E. M. V. Araldi, E. Monferrini, M. Mancino, F. Podestà, C. Scolastico, *ChemMedChem* **2009**, *4*, 615–632.
[12] F. Schumann, A. Müller, M. Koksch, G. Müller, N. Sewald, *J. Am. Chem. Soc.* **2000**, *122*, 12009–12010.
[13] S. Urman, K. Gaus, Y. Yang, U. Strijowski, N. Sewald, S. De Pol, O. Reiser, *Angew. Chem.* **2007**, *119*, 4050–4053; *Angew. Chem. Int. Ed.* **2007**, *46*, 3976–3978.
[14] D. Heckmann, A. Meyer, L. Marinelli, G. Zahn, R. Stragies, H. Kessler, *Angew. Chem.* **2007**, *119*, 3641–3644; *Angew. Chem. Int. Ed.* **2007**, *46*, 3571–3574, and references therein.
[15] A. S. M. Ressurreição, A. Bordessa, M. Civera, L. Belvisi, C. Gennari, U. Piarulli, *J. Org. Chem.* **2008**, *73*, 652–660.
[16] A. S. M. Ressurreicao, A. Vidu, M. Civera, L. Belvisi, D. Potenza, L. Manzoni, S. Ongeri, C. Gennari, U. Piarulli, *Chem. Eur. J.* **2009**, *15*, 12184–12188.
[17] M. Marchini, M. Mingozzi, R. Colombo, C. Gennari, M. Durini, U. Piarulli, *Tetrahedron* **2010**, *66*, 9528.
[18] K. L. Webster, A. B. Maude, M. E. O'Donnell, A. P. Mehrotra, D. J. Gani, *Chem. Soc. Perkin Trans. 1* **2001**, 1673–1695.
[19] C. M. Thompson, J. A. Frick, D. L. C. Green, *J. Org. Chem.* **1990**, *55*, 111–116.
[20] This procedure has been reported for the successful synthesis of 2,3-diamino propionic acid starting from serine derivatives, see: a) S. H. Rosenberg, K. P. Spina, K. W. Woods, J. Polakowski, D. L. Martin, Z. Yao, H. H. Stein, J. Cohen, J. L. Barlow, *J. Med. Chem.* **1993**, *36*, 449–459; b) I. F. Pickersgill, H. Rapoport, *J. Org. Chem.* **2000**, *65*, 4048–4057.
[21] X. Ariza, F. Urpí, C. Viladomat, J. Vilarrasa, *Tetrahedron Lett.* **1998**, *39*, 9101–9102.
[22] C. David, L. Bischoff, H. Meudal, A. Mothé, N. De Mota, S. DaNascimento, C. Llorens-Cortes, M.-C. Fournié-Zaluski, B. P. Roques, *J. Med. Chem.* **1999**, *42*, 5197–5211.
[23] V. Bavetsias, A. L. Jackman, R. Kimbell, W. Gibson, F. T. Boyle, G. M. F. Bisset, *J. Med. Chem.* **1996**, *39*, 73–85.
[24] J. M. Humphrey, R. J. Bridges, J. A. Hart, A. R. Chamberlin, *J. Org. Chem.* **1994**, *59*, 2467–2472.
[25] L. A. Carpino, A. El-Faham, F. Albericio, *J. Org. Chem.* **1995**, *60*, 3561–3564.
[26] J. Coste, E. Frérot, P. Jouin, *J. Org. Chem.* **1994**, *59*, 2437–2446.
[27] T. Shioiri, K. Ninomiya, S. Yamada, *J. Am. Chem. Soc.* **1972**, *94*, 6203–6205.
[28] Y. Fu, R. P. Hammer, *Org. Lett.* **2002**, *4*, 237–240.
[29] J.-M. Luo, C.-F. Dai, S.-Y. Lin, P.-Q. Huang, *Chem. Asian J.* **2009**, *4*, 328–335.
[30] M. De Greef, S. Abeln, K. Belkhasmi, A. Dömling, R. V. A. Orru, L. A. Wessjohann, *Synthesis* **2006**, 3997–4004.
[31] a) G. Müller, M. Gurrath, H. Kessler, *J. Comput.-Aided Mol. Des.* **1994**, *8*, 709–730; b) R. Haubner, R. Gratias, B. Diefenbach, S. L. Goodman, A. Jonczyk, H. Kessler, *J. Am. Chem. Soc.* **1996**, *118*, 7461–7472; c) R. Haubner, W. Schmitt, G. Hölzemann, S. L. Goodman, A. Jonczyk, H. Kessler, *J. Am. Chem. Soc.* **1996**, *118*, 7881–7891.
[32] F. Guarnieri, W. C. Still, *J. Comput. Chem.* **1994**, *15*, 1302–1310.
[33] W. C. Still, A. Tempczyk, R. C. Hawley, T. Hendrickson, *J. Am. Chem. Soc.* **1990**, *112*, 6127–6129.
[34] W. L. Jorgensen, D. S. Maxwell, J. Tirado-Rives, *J. Am. Chem. Soc.* **1996**, *118*, 11225–11236.
[35] The OPLS_2001 force field, among several commonly used force fields, provided the highest correlation between calculated and experimental conformational preferences within the series of cyclic RGD peptidomimetics containing diketopiperazine scaffolds with different stereochemistry and substitution at the piperazinic nitrogen atoms.
[36] MacroModel, version 9.5, Schrödinger, LLC, New York, **2007**.
[37] Glide, version 4.5, Schrödinger, LLC, New York, **2007**.

Received: February 12, 2012
Published online: April 19, 2012

 © 2012 Wiley-VCH Verlag GmbH & Co. KGaA, Weinheim